# Enhanced Adaptive Phase-Field Modeling of Brittle Fracture in Heterogeneous Materials: Integration of PHT-Splines.

*Abdel Ahad* El Mahmi [1*] , *Abdeslam* El Akkad [2] , and *Ahmed* El Khalfi [3].

[1]Research Laboratory in Science and Engineering, Faculty of Sciences and Techniques, B.P. 2202, Route Imouzzer, 30000 Fes, Morocco.
[2]Département de Mathématiques, Centre Régional des Métiers d'Éducation et de Formation de Fès-Meknès, Rue de Koweit 49, Ville Nouvelle, 30050 Fez, Morocco.
[3]Faculty of Sciences and Techniques, Organization, B.P. 2202, Route Imouzzer, 30000 Fes, Morocco.

**Abstract.** This study introduces a sophisticated adaptive phase-field model de-signed to simulate brittle fracture in heterogeneous materials. By incorporating PHT-splines, the model significantly improves the accuracy of crack propagation predictions. It effectively captures crack initiation and growth in materials with intricate microstructures, particularly enhancing precision in areas with sharp property variations. Through numerical simulations of brittle fracture in materials like ceramics, the model demonstrates its capability to accurately predict crack paths and energy dissipation during fracture. The research presents an innovative approach by integrating adaptive phase-field techniques and PHT-splines, offering a powerful tool for more precise fracture simulations in engineering contexts.

**Keywords:** Adaptive Phase-Field, Brittle Fracture, Heterogeneous Materials, PHT-Splines, Crack Propagation, Numerical Simulation.Page layout

## 1 Introduction

The advent of Isogeometric Analysis (IGA) has marked a significant breakthrough in computational mechanics by unifying the geometric exactness of Computer-Aided Design (CAD) with state-of-the-art numerical schemes for the accurate resolution of partial differential equations (PDEs).[15]. This innovative framework bridges the gap between design and analysis, providing superior geometric accuracy and numerical convergence compared to traditional Finite Element Methods (FEM) [8]. IGA's ability to leverage smooth basis functions has been particularly impactful in the field of fracture mechanics, where accurate representation of evolving discontinuities is critical [7].

Among the various methodologies developed for fracture analysis, the phase-field methodology is now firmly established as a robust paradigm for simulating fracture evolution

* Corresponding author: author@email.org

in solids, offering a thermodynamically consistent framework for simulating crack initiation, propagation, and coalescence [14]. This method circumvents the challenges of explicit crack tracking by employing an energy-based variational formulation, ensuring a natural transition between intact and fractured material states [1]. Pioneering studies have demonstrated the effectiveness of the phase-field meth-od in capturing complex fracture behaviors in Among the various computational approaches for fracture modeling, The Phase-Field Method (PFM) has established itself as a robust and thermodynamically consistent variational framework, inherent-ly capturing crack initiation, propagation, and coalescence in a unified energy-driven formulation [14]. Unlike discrete crack-tracking techniques, the phase-field approach represents fractures in a diffuse manner, enabling robust numerical treatment of complex fracture behaviors in both isotropic and anisotropic materials [21]. However, existing formulations face challenges in modeling multi-scale heterogeneous mate-rials, where microstructural variations significantly influence fracture patterns [20].

This study introduces an enhanced phase-field modeling framework tailored for brittle fracture in heterogeneous materials, integrating an advanced IGA-based discretization with PHT-Splines (Polynomial splines over Hierarchical T-meshes) [8]. Unlike conventional NURBS-based IGA [16]. which suffers from rigid refinement constraints, PHT-Splines offer adaptive local refinement while preserving the essential continuity required for higher-order phase-field formulations. This key feature allows for efficient and accurate numerical modeling of crack evolution in complex media, significantly improving computational efficiency and predictive capabilities.

## 2 Phase-field modelling

This section presents a comprehensive model to describe crack propagation in brit-tle materials based on the total energy formulation $\Psi$.

### 2.1 Total Energy Formulation

The total energy of the system is expressed in the form of the following functional:

$$\Psi = \Psi_{elas} + \Psi_{frac} - W_{ext}. \tag{1}$$

The stored elastic strain energy can be expressed as:

$$\Psi_{elas} = \int_{\Omega} g(\phi)\Psi_0(\epsilon)d\Omega. \tag{2}$$

Where:

- $g(\phi) = (1-\phi)^2$ is the degradation function, reducing elastic energy in cracked regions ($\phi = 1$).
- The function $\Psi_0(\epsilon)$ denotes the strain energy density of the undamaged (intact) material, and $\epsilon(u) = \frac{1}{2}(\nabla \mathbf{u} + \nabla \mathbf{u}^{\mathsf{T}})$ is the strain tensor.

The fracture energy is given by:

$$\Psi_{\text{frac}} = \int_{\Omega} \frac{G_c}{2}\left(\frac{\phi^2}{l_0} + \frac{l_0^4}{16}(\Delta\phi)^2 + \frac{l_0^2}{2}|\nabla\phi|^2\right) d\Omega, \tag{3}$$

where:

- The parameter $G_c$ characterizes the intrinsic resistance of a material to crack formation. It defines the minimum energy necessary to produce a unit area of new fracture surface, reflecting the toughness of the material.

- $\phi$ is the phase-field variable, it takes the value 0 in undamaged regions and gradually increases toward 1 in areas that are fully fractured. It enables a smooth transition between intact and broken material without explicitly tracking crack interfaces.
- $l_0$ defines a characteristic length scale that determines how sharply the transition occurs between the intact and damaged zones. It effectively controls the spatial resolution of the fracture zone within the numerical model.

The external work follows as:

$$W_{ext} = \int_{\Omega} \boldsymbol{f} \cdot \boldsymbol{u} d\Omega + \int_{\partial\Omega_N} t_N \cdot \boldsymbol{u} d\Gamma. \quad (4)$$

- $W_{ext}$ is determined by the external forces acting on the system, including the surface traction $t_N$ applied along the Neumann boundary $\partial\Omega_N$, and the body force f distributed throughout the domain.

## 2.2 Governing Equations

The governing equations of the phase-field model, formulated in their strong form, are derived from the variational minimization of the total energy functional, which encompasses elastic deformation, fracture energy, and applied external forces. Owing to the high-order nature of these equations, robust and accurate numerical methods are essential to ensure stability, convergence, and physical fidelity.

The subsequent section introduces the strong form in detail, establishing the mathematical basis for the weak formulation and its numerical discretization.

### *2.2.1 Mechanical Equilibrium Equation*

In the framework of crack propagation analysis, the governing equilibrium equation for the elastic field for an isotropic solid is formulated as follows:

$$-\nabla \cdot (g(\phi)\sigma) = f \ \ on \ \ \Omega. \quad (5)$$

Where:

- $\boldsymbol{\sigma}$ is the Cauchy stress tensor.
- f represents external forces acting on the material.

### *2.2.2 Phase-Field Evolution Equation*

The governing differential equation for the fourth-order phase field models could be written as:

$$\frac{G_c}{2}\left[\frac{\phi}{l_0} - \frac{l_0}{2}|\nabla\phi|^2 + \frac{l_0^3}{16}\Delta^2\phi\right] = -g'(\phi)H(x,t). \quad (6)$$

Where:

- $g'(\phi)$ : Derivative of the degradation function.

- $H(x,t) = \max_{s\in[0,t]} \Psi_e^+(\epsilon(x,s))$ represents the local strain history function at time step t, ensuring the irreversibility condition in crack evolution. The function captures the maximum positive elastic energy density $\Psi_e^+$ experienced at the integration point $x$ over the time interval s∈ [0, t], preventing crack healing and ensuring a physically consistent fracture process [14].
- In isotropic formulations, the strain energy is treated as an indivisible whole, with no distinction made between tensile and compressive contributions. Hence, $\Psi_0^-(\epsilon)$= 0 and $\Psi_0^+(\epsilon)$=$\Psi_0(\epsilon)$. Consequently, $\Psi_e(\epsilon, \phi)$ is expressed as:

$$\Psi_e(\epsilon, \phi) = g(\phi)\,\Psi_0(\epsilon). \tag{7}$$

## 2.3 Boundary Conditions

For the mechanical equilibrium equation, the elastic field is subject to Dirichlet and Neumann boundary conditions, ensuring mechanical equilibrium.

$$g(\phi)\sigma \cdot n = t_N \text{ on } \partial\Omega_N. \tag{8}$$

$$u = u_0 \text{ on } \partial\Omega_D. \tag{9}$$

- The unit outward normal vector is denoted by $n$, while $u_0$ represents the prescribed displacement at each loading step. The Dirichlet and Neumann-type boundaries are represented by $\partial\Omega_D$ and $\partial\Omega_N$, respectively, where $(\partial\Omega = \partial\Omega_N \cup \partial\Omega_D)$.

The phase-field evolution is subject to homogeneous Neumann boundary conditions imposed uniformly along the entire boundary of the domain, formally expressed as follows:

$$\Delta\phi = 0 \text{ on } \partial\Omega_D. \tag{10}$$

$$\nabla(l_0^4\Delta\phi - 2l_0^2\phi)\cdot n = 0 \text{ on } \partial\Omega_N. \tag{11}$$

## 2.4 Weak Form

### *2.4.1 Weak Form of the equilibrium Equation*

By multiplying the strong form of the equilibrium equation (5) by a test function v ∈ V, integrating over the domain Ω, and applying integration by parts (divergence theorem) along with the boundary conditions, we derive the final weak formulation:
Let the space of admissible test functions be defined as:

$V = \{\mathbf{v} \in [H^1(\Omega)]^d \mid \mathbf{v} = \mathbf{0} \text{ on } \partial\Omega_D\}$, (e.g., $d$ = 2 or 3).

Find $\mathbf{u} \in V$ such that $\forall\, \mathbf{v} \in V$ :

$$\int_\Omega g(\phi)\boldsymbol{\sigma}:\nabla\mathbf{v}\,d\Omega = \int_\Omega \mathbf{v}\cdot\mathbf{f}\,d\Omega + \int_{\partial\Omega_N} \mathbf{v}\cdot\mathbf{t}_N\,d\Gamma. \tag{10}$$

### *2.4.2 Weak Form of the Phase-Field Evolution Equation*

The weak formulation of the phase-field evolution equation (6) is derived using the Weighted Residual Method Galerkin [12], involving multiplication by a test function w ϵ W, integration

by parts over the volume, and application of homogeneous Neumann boundary conditions (10) and (11). The final form of the expression is:

Find $\phi \in \mathrm{W}$ such that $\forall\, w \in \mathrm{W}$ :

$$\int_\Omega \frac{G_c}{2}\left(\frac{\phi}{l_0}w + \frac{l_0}{2}\nabla\phi\cdot\nabla w - \frac{l_0^3}{16}\nabla\Delta\phi\cdot\nabla w\right)d\Omega = -\int_\Omega wg'(\phi)H(x,t)d\Omega. \tag{13}$$

Where:

- $\mathrm{W} = H^2(\Omega)$.
- $H(x,t)$: Irreversibility-enforcing history function.

# 3 Isogeometric discretization

## 3.1 Preliminaries of PHT-splines

PHT-splines provide an efficient and flexible framework for adaptive refinement in isogeometric analysis (IGA), serving as a generalization of B-splines over T-meshes [2]. Their hierarchical structure enables local refinement without increasing the global degrees of freedom, making them particularly suitable for application such as phase-field modeling of crack propagation in heterogeneous materials.

The initial discretization at level 0 is based on a tensor-product mesh, defined by a set of vertices:

$$U^i = \left\{\xi_1^i, \xi_2^i, \dots, \xi_{n_i+1}^i\right\},\ i \in \{1,2,3\}, \tag{14}$$

where $0 = \xi_1^i \leqslant \xi_2^i \leqslant, \dots, \leqslant \xi_{n_i+1}^i = 1$, with $n_i$ representing the number of elements in each parametric direction. The collection $U^i$ defines the initial tensor product mesh at level 0. For $d = 2$, the bi-variate tensor product mesh, $\mathbb{T}_0$ on level 0 can be expressed as:

$$\mathbb{T}_0 = \left\{ \begin{matrix} E_{0,k_\mathrm{m}} = \left[\xi_{k_1-1}^{(1)}, \xi_{k_1}^{(1)}\right] \times \left[\xi_{k_2-1}^{(2)}, \xi_{k_2}^{(2)}\right], \\ k_1 = 2, \dots, n_1+1 \text{ and } k_2 = 2, \dots, n_2+1 \end{matrix} \right\} \tag{15}$$

where, $E_{0,k_m}$ represents an element in the level-0 mesh, and the element index $k_m$ is determined by: $k_m = (k_2-2)n_1 + (k_1-1)$.

Refinement is achieved through the cross-insertion technique, where each element at level $k$ is subdivided into $2^d$ sub-elements at level $k+1$. The refinement decision is based on error estimators or gradient-based criteria, ensuring that mesh refinement is concentrated only in regions requiring increased resolution.

For numerical implementation, PHT-splines use a Bézier representation to construct basis functions efficiently in the parametric space. The set of basis functions, $N_{l,k_m}$ of polynomial degree $p$ for an element $E_{l,k_m} \in T_l$ is expressed as:

$$N_{l,k_m}\left(\xi^{(1)}, \dots, \xi^{(d)}\right) = \sum_{i_1=1}^{p+1} \cdots \sum_{i_d=1}^{p+1} C^E_{(1,\dots,i_d)(1,\dots,i_d),k_m} \hat{B} \circ \hat{\mathbf{F}}^{(E)^{-1}}\left(\xi^{(1)}, \dots, \xi^{(d)}\right) \tag{16}$$

The term $\hat{B}_{i,j}\left(\xi^{(1)}, \xi^{(2)}\right) = B_i\left(\xi^{(1)}\right)B_j\left(\xi^{(2)}\right)$ represents a tensor product of Bernstein polynomial on the reference interval $[-1;1]$and $\hat{\mathbf{F}}^{(\hat{E})}$ is employed to transform coordinates

from the reference element $[-1;1]^d$ to a physical element $E_{l,k_m} \in \mathbb{T}_I$. The coefficients $C_{i_1,\dots,i_d}$ correspond to the Bézier coefficients of the basis functions on the refined elements. Additionally, the one-dimensional Bernstein polynomials $B_{i,p}(\xi)$ are defined as:

$$B_{i,p}(\xi) = 2^{-p}\binom{p}{i-1}(1-\xi)^{p-i+1}(1+\xi)^{i-1}, \text{ where } i = 1,2,\dots,p+1. \tag{11}$$

### 3.2 Spatial discretization

A standard spatial discretization, following Galerkin's method as in [6], is utilized to approximate the field variables u and ϕ for solving the variational problem. The discretization of these variables is performed as follows:

$$u = \sum_{i=1}^{m} \mathbf{N}_i^u d_i, \text{ where } \mathbf{N}_i^u = \begin{bmatrix} N_i & 0 & \dots & 0 \\ 0 & N_i & \dots & 0 \\ \vdots & 0 & \ddots & \vdots \\ 0 & \dots & 0 & N_i \end{bmatrix}_{d\times d}, \qquad \phi = \sum_{i=1}^{m} N_i \phi_i. \tag{18}$$

Where:

- $m$ represents the number of basis functions linked to a given element.
- $N_i$ is the element shape functions corresponding to the nodes.
- $d_i$ represents the displacement degrees of freedom.
- $\phi_i$ represents the phase-field degrees of freedom.

The associated spatial derivatives for d=3 are expressed as follows:

$$\mathbf{B}_i^{\mathrm{u}} = \begin{bmatrix} N_{i,x} & 0 & 0 \\ 0 & N_{i,y} & 0 \\ 0 & 0 & N_{i,z} \\ 0.5N_{i,y} & 0.5N_{i,x} & 0 \\ 0 & 0.5N_{i,z} & 0.5N_{i,y} \\ 0.5N_{i,z} & 0 & 0.5N_{i,x} \end{bmatrix}, \ \mathbf{B}_i^{\phi} = \begin{bmatrix} N_{i,x} \\ N_{i,y} \\ N_{i,z} \end{bmatrix}. \tag{12}$$

And

$$\mathbf{H}_i^{\phi} = [\mathbf{H}_1^T \quad \mathbf{H}_2^T \quad \mathbf{H}_3^T]. \tag{20}$$

Where :

$$\mathbf{H}_1 = [\mathbf{H}_x \quad \mathbf{H}_0 \quad \mathbf{H}_0 \quad \mathbf{H}_y \quad \mathbf{H}_z \quad \mathbf{H}_0],$$
$$\mathbf{H}_2 = [\mathbf{H}_0 \quad \mathbf{H}_y \quad \mathbf{H}_0 \quad \mathbf{H}_x \quad \mathbf{H}_0 \quad \mathbf{H}_z],$$
$$\mathbf{H}_3 = [\mathbf{H}_0 \quad \mathbf{H}_0 \quad \mathbf{H}_z \quad \mathbf{H}_0 \quad \mathbf{H}_x \quad \mathbf{H}_y],$$

$$\mathbf{H}_x = [N_{i,xx} \quad N_{i,xy} \quad N_{i,xz}],$$
$$\mathbf{H}_y = [N_{i,yx} \quad N_{i,yy} \quad N_{i,yz}],$$
$$\mathbf{H}_z = [N_{i,zx} \quad N_{i,zy} \quad N_{i,zz}],$$
$$\mathbf{H}_0 = [0 \quad 0 \quad 0].$$

The strain and phase-field gradient are expressed as:

$$\varepsilon = \sum_{i=1}^{m} \mathbf{B}_i^u \mathbf{u}_i,\ \nabla\phi = \sum_{i=1}^{m} \mathbf{B}_i^\phi \phi_i. \tag{13}$$

Employing the preceding discretization scheme, the residual for the elastic field, $\boldsymbol{r_i^u}$ and the phase field, $\boldsymbol{r_i^\phi}$ are derived from the weak form of the governing equations (5) and (6) and are expressed as follows [17]:

$$r_i^u = \int_\Omega\ g(\phi)(\mathrm{B}_i^u)^T \sigma d\Omega - \int_{\partial\Omega}\ (\mathrm{N}_i^u)^T t_N dS = 0, \tag{14}$$

$$r_i^\phi = \int_\Omega \left[\frac{G_c l_0}{2}\left(\mathbf{B}_i^\phi\right)^T \nabla\phi + \frac{G_c}{l_0} N_i\phi + \frac{G_c l_0^3}{16}\left(H_i^\phi\right)^T \nabla\phi\right] d\Omega + \int_\Omega g'(\phi)H(x,t)d\Omega = 0. \tag{15}$$

The stiffness matrix, on elemental level, for the displacement, $K_{ij}^{uu}$ and the phase field, $K_{ij}^{\phi\phi}$ are:

$$K_{ij}^{\mathrm{uu}} = \frac{\partial r_{i,e}^{\mathrm{u}}}{\partial u_j} = \int_\Omega\ g(\phi)(\mathrm{B}_i^u)^T \mathrm{C}_e\left(\mathrm{B}_j^{\mathrm{u}}\right) d\Omega, \tag{24}$$

$$K_{ij}^{\phi\phi} = \frac{\partial r_{i,e}^{\phi}}{\partial \phi} = \int_\Omega \frac{G_c l_0}{2}\left(\mathrm{B}_i^\phi\right)^T \left(\mathbf{B}_j^\phi\right) d\Omega + \int_\Omega \left(\left[\frac{G_c}{l_0} + g''(\phi)H(x,t)\right] N_i N_j + \frac{G_c l_0^3}{16}\left(H_i^\phi\right)^T \left(H_i^\phi\right)\right) d\Omega. \tag{25}$$

For a three-dimensional model, the fourth-order elasticity tensor $\mathrm{C}_e$ is expressed as:

$$\mathrm{c_E} = \frac{E}{(1+\nu)(1-2\nu)} \begin{bmatrix} (1-\nu) & \nu & \nu & 0 & 0 & 0 \\ \nu & (1-\nu) & \nu & 0 & 0 & 0 \\ \nu & \nu & (1-\nu) & 0 & 0 & 0 \\ 0 & 0 & 0 & (0.5-\nu) & 0 & 0 \\ 0 & 0 & 0 & 0 & (0.5-\nu) & 0 \\ 0 & 0 & 0 & 0 & 0 & (0.5-\nu) \end{bmatrix}, \tag{16}$$

where E denotes the material's elastic modulus and ν represents Poisson's ratio.

Equations (24) and (25) are solved subject to the boundary conditions dictated by the selected phase-field model. The prescribed displacement is enforced along the Dirichlet boundary $\partial\Omega_D$, and the corresponding external force, $\mathrm{F^u}$ is computed through the virtual work associated with the active basis functions.

The displacement $u$ is subsequently computed as:

$$u = (K^{uu})^{-1} F^u. \tag{27}$$

This study employs a cubic degradation function $g(\phi)$ instead of the conventional quadratic form. As a result, its derivative $g'(\phi)$ introduces nonlinearity into the governing equation (23), which is solved through nested iterations using the Newton–Raphson method.

The Newton-Raphson method for solving a general equation $f(\phi) = 0$ is given by the iterative update:

$$\phi^{(k+1)} = \phi^{(k)} - \frac{f\left(\phi^{(k)}\right)}{f'\left(\phi^{(k)}\right)} \tag{28}$$

In our context, $f(\phi)$ is related to the derivative of the degradation function $g'(\phi)$. To circumvent potential instability arising from linearized solutions in the staggered scheme,

we replace $g''(\phi)$ with an approximation derived from a Taylor series expansion around a point $\phi_2 \epsilon [0;1]$. This approximation is expressed as:

$$g'(\phi_1) = g'(\phi_2) + g''(\phi_2)(\phi_1 - \phi_2) + \frac{g'''(\phi_2)}{2}(\phi_1 - \phi_2)^2 + \cdots, \quad (29)$$

assuming $\phi_1 = 1$, which implies $g'(\phi_1) = 0$, and neglecting higher-order terms, we obtain:

$$0 \approx g'(\phi) + g''(\phi)(1 - \phi). \quad (30)$$

Hence, $g''(\phi)$ is approximated by:

$$g''(\phi) = -\frac{g'(\phi)}{1-\phi}, \text{ for } \phi \neq 1. \quad (31)$$

The phase field equation is solved separately as:

$$\phi = (\mathbf{K}^{\phi\phi})^{-1}\mathbf{F}^{\phi}. \quad (32)$$

At the elemental level, the expression for $F^{\phi}$ is derived as:

$$F_i^{\phi} = \int_{\Omega} g''(\phi) N_i H(\boldsymbol{x}, t) d\Omega. \quad (33)$$

## 4 The numerical experiments

This study analyzes the mode-I fracture behavior of a 2D cantilever beam using the fourth-order phase-field model with a cubic stress-degradation function. The beam, with an initial crack of 0.5 mm, is subjected to incremental displacement loading of $\boldsymbol{\Delta u} = 0.6 \times \mathbf{10^{-6}}$ mm per step. The material properties are E = $100 \times \mathbf{10^3}$ N/$\boldsymbol{mm^2}$, $\boldsymbol{\nu}$ = 0.3, and$\boldsymbol{G_c}$= $0.01\times \mathbf{10^{-3}}$kN/mm. An adaptive h-refinement scheme is applied with mesh sizes h $\approx$ 0.25 $\boldsymbol{l_0}$ and h $\approx$ 0.5 $\boldsymbol{l_0}$, where $\boldsymbol{l_0}$ = 0.015 mm. The critical loads recorded are 3.5 kN for h ≈ 0.5 $\boldsymbol{l_0}$ and 3.52 kN for h ≈ 0.25 $\boldsymbol{l_0}$, with only 0.5% deviation. The force-displacement response and crack evolution confirm that h ≈ 0.5 $\boldsymbol{l_0}$is sufficient, ensuring accuracy while optimizing computational efficiency.

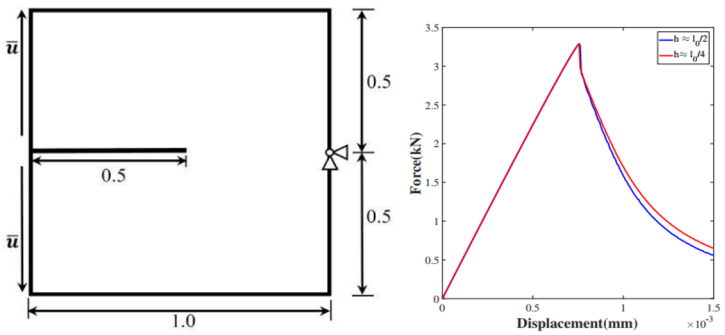


**Fig.1.** Cantilever beam under tension.

In this figure, (a) shows the geometrical setup and boundary conditions, with all dimensions in mm, (b) displays the force-displacement curves obtained using adaptive h-refinement with the fourth-order phase-field model and cubic stress degradation, simulated for h ≈ 0.5 $l_0$ and h ≈ 0.25 $l_0$, with $l_0$ = 0.015 mm.

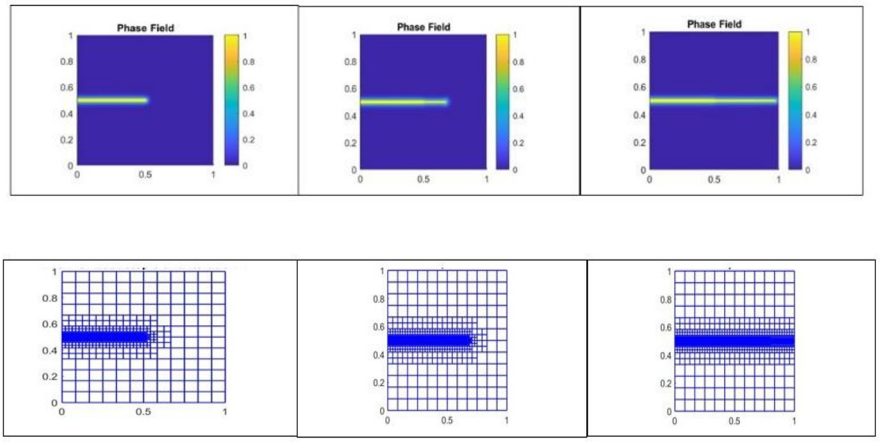


**Fig.2.** Crack Pattern and Mesh Refinement of cantilever beam.

The simulation is performed using an adaptive h-refinement scheme, incorporating the fourth-order phase-field model with a cubic stress-degradation function. The computational setup is defined by a characteristic length scale of $l_0$ = 0.015 mm and element size h ≈ 0.5 $l_0$. The results highlight the crack propagation process and the effectiveness of mesh refinement in capturing fracture evolution with high accuracy.

## 5 Conclusion

This study presents an advanced phase-field framework for fourth-order models, integrating IGA and PHT-splines to enhance numerical accuracy, geometric fidelity, and computational stability. A refined weak formulation was derived, ensuring a consistent representation of elastic and fracture energy contributions. The use of PHT-splines enabled local refinement while maintaining $C^1$-continuity, improving solution accuracy and efficiency. An optimized Newton-Raphson solver ensured stable convergence, and benchmark validations confirmed the model's effectiveness in predicting crack initiation and propagation.

**Acknowledgments**. The authors gratefully acknowledge the insightful comments and constructive critiques provided by the anonymous reviewers. Their careful assessment and thoughtful recommendations have significantly contributed to improving the clarity, rigor, and overall quality of this manuscript.

## References

1. M. Ambati, T. Gerasimov, and L. De Lorenzis, "A review on phase-field models of brittle fracture and a new fast hybrid formulation," Computational Mechanics, vol. 55, no. 2, pp. 383–405, 2015.

2. C. Anitescu, M. N. Hossain, and T. Rabczuk, "Recovery-based error estimation and adaptivity using high-order splines over hierarchical T-meshes," Computer Methods in Applied Mechanics and Engineering, vol. 328, pp. 638–662, 2018.
3. M. J. Borden, T. J. Hughes, C. M. Landis, and C. V. Verhoosel, "A higher-order phase-field model for brittle fracture: Formulation and analysis within the isogeometric analysis framework," Computer Methods in Applied Mechanics and Engineering, vol. 273, pp. 100–118, 2014.
4. M. J. Borden, M. A. Scott, J. A. Evans, and T. J. Hughes, "Isogeometric finite element data structures based on Bézier extraction of NURBS," International Journal for Numerical Methods in Engineering, vol. 87, no. 1–5, pp. 15–47, 2011.
5. C. L. Chan, C. Anitescu, and T. Rabczuk, "Volumetric parametrization from a level set boundary representation with PHT-splines," Computer-Aided Design, vol. 82, pp. 29–41, 2017.
6. J. A. Cottrell, T. J. Hughes, and Y. Bazilevs, Isogeometric Analysis: Toward Integration of CAD and FEA. Wiley, 2009.
7. L. De Lorenzis and C. Maurini, "Phase-field modeling of brittle fracture: A review," Archives of Computational Methods in Engineering, vol. 28, no. 3, pp. 1001–1040, 2021.
8. J. Deng, F. Chen, X. Li, C. Hu, W. Tong, Z. Yang, and Y. Feng, "Polynomial splines over hierarchical T-meshes," Graph. Models, vol. 75, no. 6, pp. 301–312, 2013.
9. G. A. Francfort and J. J. Marigo, "Revisiting brittle fracture as an energy minimization problem," Journal of the Mechanics and Physics of Solids, vol. 46, no. 8, pp. 1319–1342, 1998.
10. S. Goswami, C. Anitescu, and T. Rabczuk, "Adaptive fourth-order phase field analysis for brittle fracture," Computer Methods in Applied Mechanics and Engineering, vol. 361, p. 112808, 2020.
11. A. A. Griffith, "The phenomena of rupture and flow in solids," Philosophical Transactions of the Royal Society of London. Series A, vol. 221, no. 582–593, pp. 163–198, 1921.
12. O. Gultekin, H. Dal, and G. A. Holzapfel, "Numerical aspects of anisotropic failure in soft biological tissues favor energy-based criteria: A rate-dependent anisotropic crack phase-field model," Computer Methods in Applied Mechanics and Engineering, vol. 331, pp. 23–52, 2018.
13. V. Hakim and A. Karma, "Laws of crack motion and phase-field models of fracture," Journal of the Mechanics and Physics of Solids, vol. 57, no. 2, pp. 342–368, 2009.
14. C. Miehe, M. Hofacker, and F. Welschinger, "A phase field model for rate-independent crack propagation: Robust algorithmic implementation based on operator splits," Computer Methods in Applied Mechanics and Engineering, vol. 199, no. 45–48, pp. 2765–2778, 2010.
15. V. P. Nguyen, C. Anitescu, S. P. A. Bordas, and T. Rabczuk, "Isogeometric analysis: An overview and computer implementation aspects," Mathematics and Computers in Simulation, vol. 117, pp. 89–116, 2015.
16. L. E. Ouadefli, O. E. Moutea, A. E. Akkad, A. Elkhalfi, S. Vlase, and M. L. Scutaru, "Mixed isogeometric analysis of the Brinkman equation," Mathematics, vol. 11, no. 12, Art. no. 2750, 2023.

17. J. M. Sargado, E. Keilegavlen, I. Berre, and J. M. Nordbotten, "High-accuracy phase-field models for brittle fracture based on a new family of degradation functions," Journal of the Mechanics and Physics of Solids, vol. 111, pp. 458–489, 2018.
18. M. L. Scutaru, S. Guendaoui, L. E. Ouadefli, O. Koubaiti, A. El Akkad, A. Elkhalfi, and S. Vlase, "Flow of Newtonian Incompressible Fluids in Square Media: Isogeometric vs. Standard Finite Element Method," Mathematics, vol. 11, no. 17, p. 3702, 2023.
19. T. W. Sederberg, J. Zheng, A. Bakenov, and A. Nasri, "T-splines and T-NURCCs," ACM Transactions on Graphics (TOG), vol. 22, no. 3, pp. 477–484, 2003.
20. C. V. Verhoosel and R. de Borst, "A phase-field model for cohesive fracture," International Journal for Numerical Methods in Engineering, vol. 96, no. 1, pp. 43–62, 2013.
21. J. Y. Wu, V. P. Nguyen, C. T. Nguyen, D. Sutula, S. Sinaie, and S. P. A. Bordas, "Phase-field modeling of fracture in anisotropic brittle solids," Int. J. Solids Struct., vol. 191–192, pp. 434–451, 2020.